Optical detection of CH_3 during diamond chemical vapor deposition

D. G. Goodwin and N. G. Glumac
Division of Engineering and Applied Science
California Institute of Technology M/C 104-44
Pasadena, CA 91125

E. J. Corat
Instituto Nacional de Pesquisas Espaciais
Sao Jose dos Campos
SP Brazil

ABSTRACT

Measurements of CH_3 have been made using resonance-enhanced multiphoton ionization (REMPI) in two different diamond growth environments. Spatial profiles of methyl above the substrate have been measured in a filament-assisted reactor, which show that the CH_3 concentration is depleted near the substrate. The CH_3 concentration at the substrate shows an approximate Arrhenius dependence on substrate temperature below 1000 K, characterized by an activation energy of 4 kcal/mole. Methyl measurements were also made in a 35 Torr hydrogen/oxygen flame into which methane is injected near the substrate. Radial profiles of methyl, acquired using REMPI, and of CH_4, acquired using sampling mass spectroscopy, are in good qualitative agreement with the results of numerical simulations.

1. INTRODUCTION

Experimental studies [1–8] point to the methyl radical CH_3 as the dominant precursor to diamond during chemical vapor deposition (CVD). For this reason, *in situ* diagnostic methods which can detect methyl are very useful for understanding the complex radical chemistry and transport 0 under diamond CVD conditions.

The first *in situ* detection of CH_3 during diamond growth was made by Celii *et al.* using infrared diode laser absorption spectroscopy [9] and later resonance-enhanced multiphoton ionization (REMPI) [10] in a filament-assisted reactor. Although the absorption measurements are easier to quantify, their line-of-sight nature can make the comparison with numerical simulations difficult [11]. On the other hand, the REMPI technique, which is more difficult to extract absolute concentrations from, is well-suited to measuring spatially-resolved relative concentration profiles, which may easily be compared with numerical model predictions.

We have used REMPI to probe methyl in two different diamond deposition environments. Spatial profiles of CH_3 as a function of distance normal to the substrate were measured in a filament-assisted reactor, and the role of the substrate temperature on the CH_3 concentration at the substrate was examined in detail. We have also used REMPI to detect CH_3 in a novel flame method for diamond growth, in which methane is injected into a low-pressure hydrogen/oxygen flame near the substrate.

2. FILAMENT-ASSISTED DIAMOND GROWTH

2.1 Experimental

The reactor used for the filament-assisted work is described in more detail elsewhere [12]. Briefly, it consists of a 2.0 inch OD five-way cross with water-cooled walls. Before beginning the optical measurements, continuous diamond films are grown for 24 hours using a gas mixture of 0.5% CH_4 in H_2. The substrates are electrically-heated molybdenum foils (5 mm × 20 mm × 125 μm).

The laser beam for the REMPI measurements is generated by frequency-doubling the output of a YAG-pumped pulsed dye laser, yielding pulses of approximately 1 mJ near the CH_3 two-photon $3p^2A_2'' \leftarrow X^2A_2''$ (0-0) Q-branch transition at 333.5 nm. The UV beam is focused into the reactor through calcium fluoride windows using either a 20 cm or 50 cm fused silica lens.

When the laser wavelength coincides with the $3p^2A_2'' \leftarrow X^2A_2''$ (0-0) transition, photoelectrons are generated due to ionization out of the upper state. These photoelectrons are collected by a biased platinum probe wire (250 μm diameter) located approximately 1.5 mm above the laser beam waist. A small spherical bead is formed at the end of the wire with an arc welder, in order to provide a well-defined electric field at the probe tip. Due to the strong intensity dependence of the REMPI process, most of the ionization occurs within the beam waist, providing sub-mm spatial resolution normal to the substrate, and several-mm resolution parallel to the substrate. The laser beam is aligned colinear with the long dimension (20 mm)

0-8194-1417-4/94/$6.00

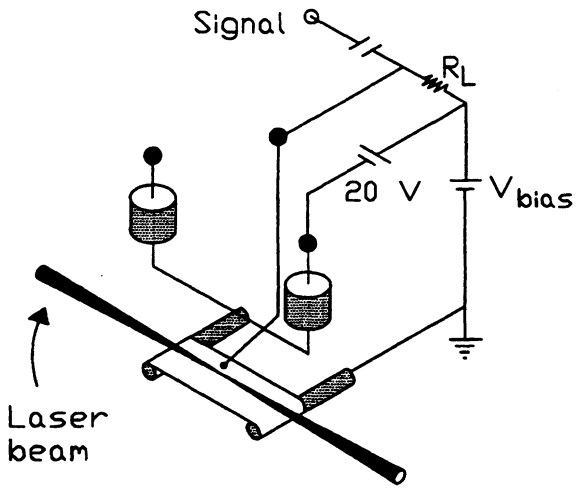

Figure 1: Schematic of experimental geometry and biasing scheme for filament-assisted studies.

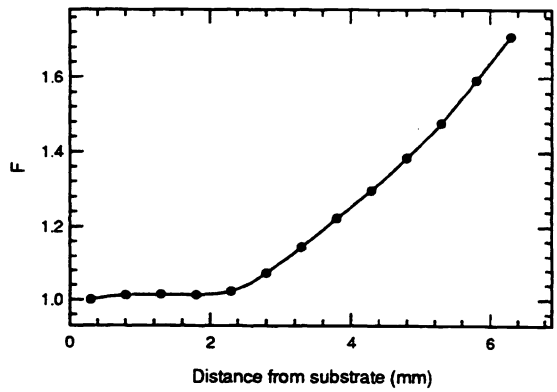

Figure 2: Measured correction factor for electron collection efficiency, normalized to the value at the substrate.

of the substrate, and therefore gradients of CH_3 along the beam waist are expected to be minimal.

The entire reactor may be translated with respect to the stationary laser beam in the direction normal to the substrate. The ionization probe enters the reactor through a sliding feed-through, and is rigidly mounted outside the reactor so that it remains fixed relative to the laser beam as the reactor is translated.

The substrate could be brought to within ≈ 0.3 mm of the laser focus before clipping of the beam occurred (detected by a sudden increase in ionization signal). Since modeling studies [11] have shown that the chemical mean free path of CH_3 is approximately 1 mm under filament-assisted conditions, we expect the methyl concentration at 0.3 mm from the substrate to be essentially the same as that at the film surface.

The geometry of the substrate, filament, and laser beam is shown along with the biasing scheme in Figure 1. The substrate is grounded and the filament is positively biased at 20 V less than the ionization probe potential, which was set at +100 V. We found that this value resulted in saturated electron collection for various experimental conditions. The ionization signal is acquired with a gated integrator, using a gate width of 100 ns.

The filament consists of a single, straight 200 μm diameter tungsten wire, approximately 25 mm long, and for the measurements reported here was kept 11 mm from the substrate. The filament brightness temperature is measured through a glass viewport on a side arm using a one-color disappearing-filament pyrometer.

All results presented here were obtained for a pressure of 35 mbar.

2.2 Data Reduction

We assume the methyl concentration at the laser focus may be related to the measured charge S induced on the ionization probe as follows, assuming constant laser energy:

$$[CH_3] \propto FSQ_{vib} \tag{1}$$

where F is a position-dependent correction factor, defined as

$$F = eN/S, \tag{2}$$

where N is the number of generated photoelectrons. Q_{vib} is the vibrational partition function, which enters since only the vibronic ground state is detected. We do not apply a rotational partition function correction, since many rotational levels of the rotationally-unresolved Q branch are simultaneously pumped, and we find experimentally that the shape of the Q branch has little temperature dependence over the temperature range of interest here.

The correction factor F differs from unity due to electrostatic effects, since the gate width is chosen to be short enough that only electrons are collected. The potential induced on the probe due to the cloud of positive ions left behind results in the induced charge being smaller than eN. It may be shown that [13, 14]

$$S = eN\frac{\Delta V}{V_{bias}} \tag{3}$$

where ΔV is the potential difference between the laser focus and the probe, and V_{bias} is the potential applied between the probe and substrate. Since ΔV will change somewhat as the substrate and filament are translated with respect the the stationary laser beam and probe, $F(x) = eN/S = V_{bias}/\Delta V$ will depend on position.

The correction factor was measured experimentally, by introducing a small amount (1%) of argon into the H_2/CH_4 mixture, and monitoring the REMPI signal from the nearby

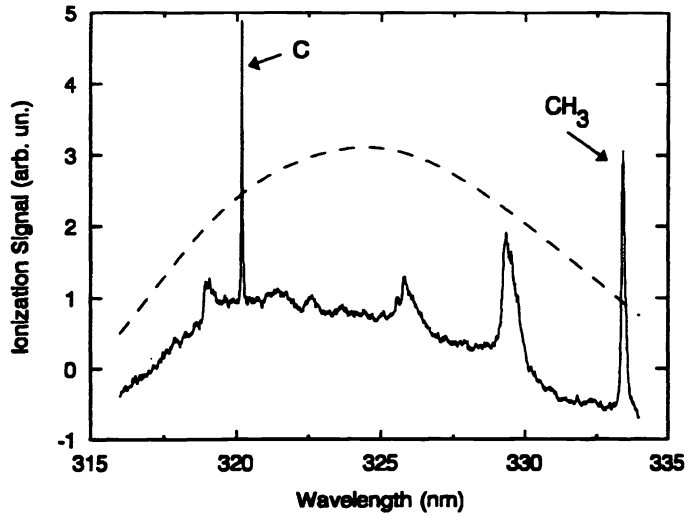

Figure 3: Ionization spectrum obtained 0.5 mm above the substrate for T_{sub} = 1000 K. The dashed line shows the measured relative laser energy.

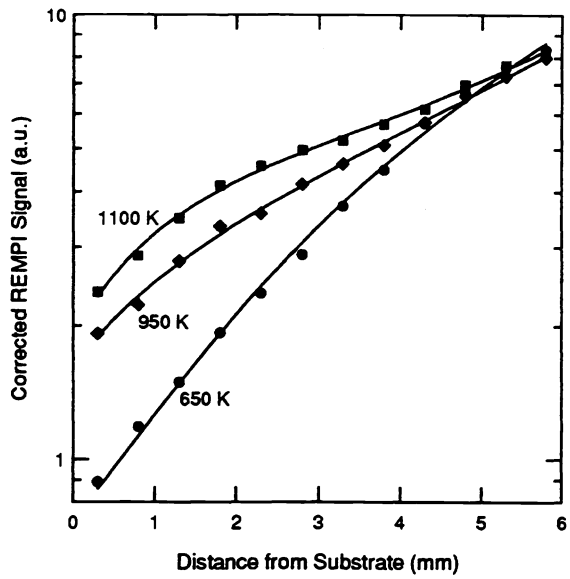

Figure 4: Relative concentration of the vibronic ground state of CH_3 vs. distance from substrate for three substrate temperatures.

argon (3+1) $4s'$ REMPI transition at 314.4 nm as a function of position at room temperature with the filament off. The pressure was reduced to match the density during the actual measurements. Since in this case the argon concentration must be constant, the Ar REMPI signal is a direct measure of $1/F$. The correction factor so determined is shown in Figure 2.

2.3 Results

A typical survey ionization spectrum is shown in Figure 3. This spectrum was obtained at the substrate under normal diamond growth conditions, with a substrate temperature of 1000 K. In addition to the CH_3 REMPI transition at 333.5 nm, a peak due to photolytically-produced C (^{1}D) at 320.2 nm is seen [10], as well as several broad peaks. The variation in laser energy is shown by the dashed curve in this figure. All results below are obtained at the peak of the CH_3 REMPI band, corrected for background ionization.

The measured REMPI signal, corrected for electron collection efficiency, is shown in Figure 4 as a function of distance from the substrate. These profiles are proportional to the population in the vibronic ground state. No partition function correction was applied to this data to estimate the total CH_3 concentration, since the temperature profile has not yet been measured.

These results show that the methyl concentration decreases as the substrate is approached. This is not surprising, since the CH_3 concentration was observed by Celii *et al.* to decrease sharply with increasing distance from the

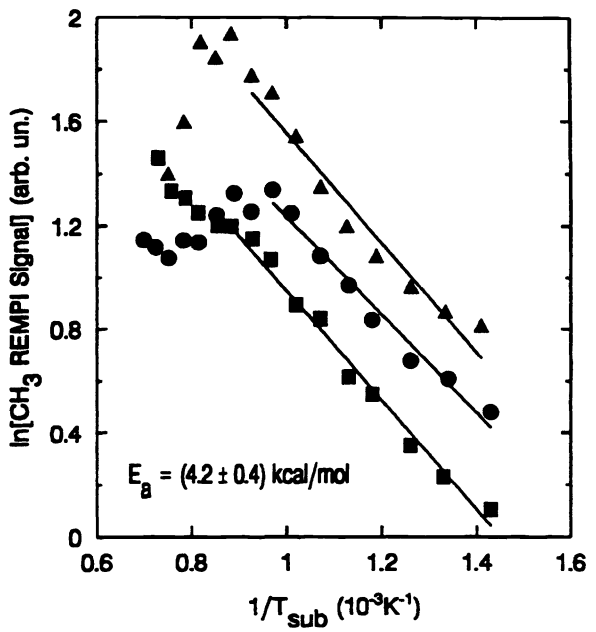

Figure 5: Arrhenius plot of relative CH_3 concentration at the substrate vs. T_{sub}.

filament (here at 11 mm) [10]. The measurements of Celii *et al.* were at a fixed distance from the substrate (~ 4 mm) at a fixed substrate temperature. The surprising result of the present measurements is the effect of substrate temperature. Beyond ~ 5 mm from the substrate, the signal is independent of substrate temperature. However, closer to the substrate the signal falls off more rapidly at lower substrate temperatures than at higher ones.

In Figure 5, the REMPI signal measured at the substrate, corrected by Q_{vib}, is plotted in Arrhenius form vs. substrate temperature. At temperatures below about 1000 K, the data fall on reasonably straight lines, and can all be described by an activation energy of approximately 4 kcal/mole. We may compare this value to reported activation energies for the diamond growth rate. Kondoh *et al.* [15] have measured growth rates which peak at about 1200 K, and decline for higher temperatures. They report an activation energy in the temperature range of 1000–1200 K of 22–24 kcal/mole. Chu *et al.* [16] have measured the homoepitaxial growth rates on (100), (111), and (110) faces over the temperature range of 950–1250 K. They report activation energies of 8, 12, and 18 kcal/mole for homoepitaxial growth on the (100), (111), and (110) faces, respectively, although the temperature dependence appears to be larger in the range 950–1000 K, and they assign an activation energy of 50 kcal/mole in this region. This comparison indicates that the temperature dependence of the methyl radical concentration at the surface contributes to the measured activation energies for growth, but is less important than other factors.

Preliminary modeling studies indicate that the most likely cause of the enhanced fall-off at low substrate temperatures is gas-phase recombination of CH_3 through the reactions

$$CH_3 + CH_3 \rightarrow C_2H_6 \quad (4)$$

and

$$CH_3 + H \rightarrow CH_4. \quad (5)$$

These reactions have pressure-dependent rate constants with negative temperature exponents (faster at lower temperature) [17, 18]. Using rate constants appropriate for 35 mbar and estimated mole fractions based on the measurements of Hsu [19] for a similar filament-assisted experiment, we find that these two reactions contribute almost equally to methyl consumption in this temperature range. We estimate that the methyl destruction time, considering both reactions, is 200 μs at 700 K, while at 1400 K it is an order of magnitude longer (2 ms).

It is also possible that CH_3 could recombine heterogeneously on the diamond surface. We are currently carrying out 2-D simulations using the computational fluid dynamics model discussed below to try to understand this temperature dependence.

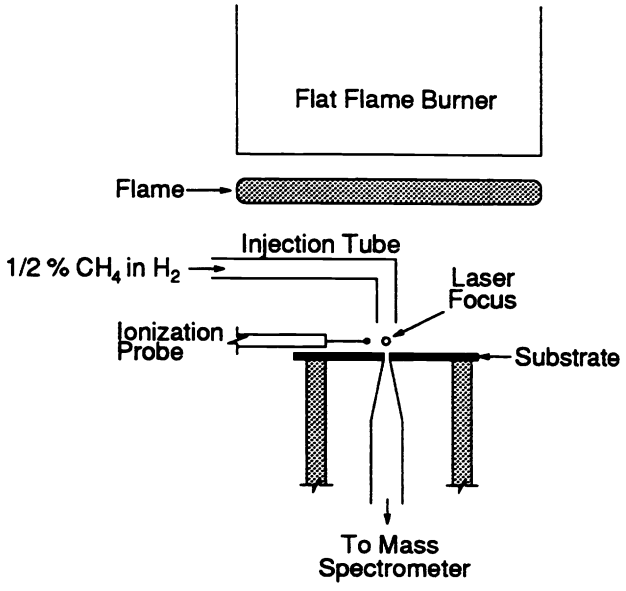

Figure 6: Experimental setup for diamond growth and diagnostics in hydrogen/oxygen flames.

3. H_2/O_2 FLAMES WITH CH_4 INJECTION

We have recently demonstrated that diamond may be grown by injecting methane near a substrate immersed in a low-pressure hydrogen/oxygen flame [20, 21]. We have also used REMPI in this environment to better understand the mixing and reaction between the injected gas jet and the surrounding flame.

3.1 Experimental

The experimental setup, shown in Figure 6, consists of a low-pressure flat flame burner (6 cm diameter) designed specifically for diamond growth studies. The burner is described in more detail elsewhere [22]. The burner and substrate are contained in a stainless steel bell-jar vacuum chamber, which is equipped with quartz viewports to allow optical diagnostic measurements. Commercial grade gases are provided from bottles and metered by electronic mass flow controllers. The gases are thoroughly mixed before entering the chamber.

For this work, slightly rich (ϕ = 1.25 to 1.5) hydrogen/oxygen flames are run at 35 Torr, with an unburned gas velocity at the burner of about 75 cm/s. A flow of 200 sccm of 0.5% CH_4 in H_2 is injected perpendicular to the substrate through a 1.7 mm ID alumina tube, resulting in a gas velocity at the tube exit 1 mm above the substrate of about 100 m/s. The temperature of the injected gas is estimated to be about 800 °C. Using kinetic theory estimates for the gas viscosity, we estimate a Reynolds number of $\approx$ 10 for the injected flow based on the tube diameter. Thus, we expect that the flowfield is laminar.

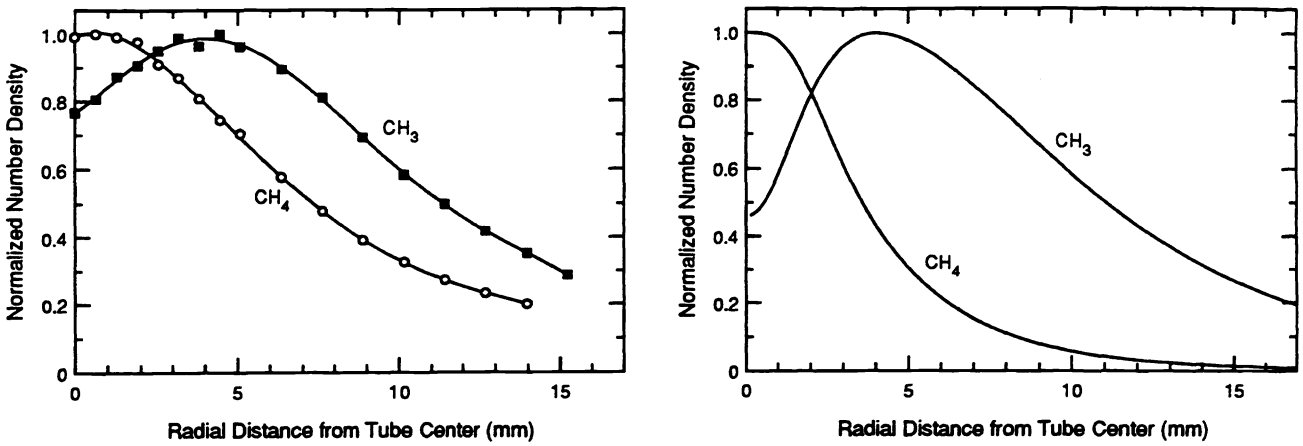

Figure 7: Measured (left) and predicted (right) CH_3 and CH_4 radial profiles at the substrate. All curves are normalized to their respective maxima.

A silicon substrate is used, which is heated by contact with a resistively-heated molybdenum strip. The substrate is prepared by scratching with 1 micron diamond paste before deposition. Well-faceted diamond is observed to grow on the substrate near the injection tube [20].

The injection tube is mounted on a horizontal translation feedthrough. By scanning the tube past the measurement position, radial profiles of CH_3 are acquired using REMPI. In addition, the gas at the substrate is sampled through a small hole in the substrate by a quartz probe and analyzed with a quadrupole mass spectrometer, to determine stable species concentrations. The probe orifice diameter is ≈ 0.2 mm, which based on previous studies [23] should yield a spatial resolution of ≈ 0.5 mm. The probe pressure is kept at 0.5 torr to rapidly quench chemistry other than radical recombination. The sampling procedure is similar to that used previously by Harris, Weiner and Perry [24] in their study of filament-assisted diamond growth.

For the REMPI measurements, we estimate that ionization takes place over roughly 5 mm along the beam waist. Since the injection tube diameter is less than this, our measured methyl profiles are not fully spatially resolved, particularly near the axis. In principle, an Abel inversion could be applied to estimate the true radial CH_3 profile, but this has not been done here.

The laser beam is focused approximately 0.5 mm above the substrate surface. The ionization probe is placed adjacent to the laser focus approximately 1-2 mm away. The probe bias voltage (100 V) is chosen to obtain saturated electron collection without significant secondary ionization. Since the injection tube is an electrical insulator, there is little perturbation of the electric field near the probe as the tube is translated, and therefore we assume the REMPI collection efficiency is constant. Since the gas temperature at the measurement location is also approximately constant, the profile with radial distance of the REMPI signal, corrected for the nonresonant background, can be interpreted as a relative CH_3 concentration profile (averaged, however, over the laser focus).

3.2 Results

Relative concentration profiles of CH_4 obtained by mass spectrometry and CH_3 obtained by REMPI are shown in Figure 7. The CH_3 concentration is seen to peak at larger radii than the CH_4 concentration, which is largest at the injection tube centerline. Since methyl is produced by the fast bimolecular reaction

$$CH_4 + H \rightleftharpoons CH_3 + H_2, \qquad (6)$$

the methyl concentration should scale approximately as $[CH_3] \propto [CH_4][H]$, which, since H must diffuse from outside the jet toward the center, will produce a methyl radial profile like that seen in Figure 7. Methyl remains above 30% of its maximum value out to 15 mm from the injection jet while deposit radii are always less than 3 mm. This indicates that the lack of diamond growth at radial distances beyond 3 mm is probably not due to lack of growth species or H atom concentration, but rather to oxidation.

Attempts were made to detect C_2H_2 and C_2H_4, but their concentrations were below the detection limits of our mass spectrometer. From this, we can estimate an upper bound on the acetylene mole fraction at the substrate of 2×10^{-5}. The low acetylene concentration at the substrate indicates the degree of control over the chemical composition of the gas at the substrate which is possible with this method, unlike most other diamond CVD techniques where the hydrocarbon gases pass through the activation region.

To model the flow region around the injection jet and near the substrate, a commercial 3-D computational fluid

dynamics (CFD) code (FLUENT [25]) with limited kinetic modeling capability was used. FLUENT solves the momentum, energy, and species conservation equations to yield the velocity, temperature, and concentration fields throughout the domain. For the present simulations, we use estimated diffusion coefficients, viscosity, and thermal conductivity, all assumed to be constant. The flow was modeled as a 2-D axisymmetric jet impinging on an infinite substrate. The post-flame gas composition was calculated using a 1-D flame code, and used as input to FLUENT. The other inputs were chosen to match experimental parameters.

In this simplified problem, the chemistry is confined to reaction (6) (both forward and reverse directions), plus recombination via reaction (5). The reverse of reaction (5) is neglected since its contribution for the temperatures and concentrations of the posed problem is negligible compared with the forward rate of reaction (6).

Results for the calculated normalized radial profiles of CH_4 and CH_3 at the surface are also shown in Figure 7. The qualitative agreement between model and experiment is good, although the calculated CH_4 profile falls off somewhat more rapidly than that measured, which may be due to the approximate transport properties and reaction rates used in the simulation. For CH_3, the lack of complete spatial resolution near $r = 0$ may also contribute to the disagreement at small radii between model and experiment.

4. SUMMARY

Resonance-enhanced multiphoton ionization has been used to measure spatial profiles of CH_3 in two different diamond growth environments. In the filament-assisted case, a distinct fall-off is found as the substrate is approached, which is enhanced at lower substrate temperatures. At low substrate temperature, it appears that recombination of CH_3 in the cool gas layer near the substrate or on the surface is responsible for this enhanced fall-off. In hydrogen/oxygen flames with methane addition, radial profiles of CH_3 have been acquired which are in qualitative agreement with the results of numerical simulation.

5. ACKNOWLEDGMENTS

This work has been supported, in part, by the National Science Foundation under Grant CTS-9057921 and by the Office of Naval Research, under contract N00014-90-J-1386. An additional equipment grant from the AT&T Foundation is gratefully acknowledged.

6. REFERENCES

1. C. J. Chu, M. P. D'Evelyn, R. H. Hauge, and J. L. Margrave, J. Mater. Res. **5**, 2405 (1990).
2. C. J. Chu, M. P. D'Evelyn, R. H. Hauge, and J. L. Margrave, J. Appl. Phys. **70**, 1695 (1991).
3. M. P. D'Evelyn, C. J. Chu, R. H. Hauge, and J. L. Margrave, J. Appl. Phys. **71**, 1528 (1992).
4. S. J. Harris and A. M. Weiner, Thin Solid Films **212**, 201 (1992).
5. S. J. Harris and A. M. Weiner, J. Appl. Phys. **70**, 1385 (1991).
6. L. R. Martin and M. W. Hill, J. Mater. Sci. Lett. **9**, 621 (1990).
7. S. J. Harris and L. R. Martin, J. Mater. Res. **5**, 2313 (1990).
8. C. E. Johnson, W. A. Weimer, and F. M. Cerio, J. Mater. Res. **7**, 1427 (1992).
9. F. G. Celii, P. E. Pehrsson, H. t. Wang, and J. E. Butler, Appl. Phys. Lett. **52**, 2043 (1988).
10. F. G. Celii and J. E. Butler, J. Appl. Phys. **71**, 2877 (1992).
11. D. G. Goodwin and G. G. Gavillet, J. Appl. Phys. **68**, 6393 (1990).
12. E. J. Corat and D. G. Goodwin, J. Appl. Phys. **74**, 2021 (1993).
13. T. A. Cool, Applied Optics **23**, 1559 (1984).
14. B. B. Rossi and H. H. Staub, *Ionization Chambers and Counters* (Academic Press, New York, 1949).
15. E. Kondoh, T. Ohta, T. Mitomo, and K. Ohtsuka, Appl. Phys. Lett. **59**, 488 (1991).
16. C. J. Chu, R. H. Hauge, J. L. Margrave, and M. P. D'Evelyn, Appl. Phys. Lett. **61**, 1393 (1992).
17. J. Warnatz, in *Combustion Chemistry*, edited by W. C. Gardiner, Jr. (Springer-Verlag, New York, 1984), p. 197.
18. C. J. Cobos and J. Troe, Zeitsch. Phys. Chem. Neue Folge **167**, 129 (1990).
19. W. L. Hsu, J. Appl. Phys. **72**, 3102 (1992).
20. N. G. Glumac and D. G. Goodwin, Appl. Phys. Lett. **60**, 2695 (1992).

21. N. G. Glumac, E. J. Corat, and D. G. Goodwin, Diamond and Related Materials **2**, 169 (1993).

22. N. G. Glumac and D. G. Goodwin, Thin Solid Films **212**, 122 (1992).

23. S. J. Harris, A. M. Weiner, R. J. Blint, and J. E. M. Goldsmith, in *Twenty-first Symposium (International) on Combustion* (The Combustion Institute, Pittsburgh, PA, 1986), p. 1033.

24. S. J. Harris, A. M. Weiner, and T. A. Perry, Appl. Phys. Lett. **53**, 1605 (1988).

25. Fluent Inc., Centerra Resources Park, 10 Cavendish Court, Lebanon, NH.